Int. J. Multiphase Flow Vol. 9, No. 5, pp. 463–489, 1983
Printed in Great Britain.

0301-9322/83 $3.00 + .00
Pergamon/Elsevier

STOCHASTIC CHARACTERISTICS OF VAPOR FRACTION AND WALL PRESSURE FLUCTUATIONS IN BOILING FLOWS†

PARVEEN K. JAIN
Systems Control Inc., Palo Alto, CA 94304, U.S.A.

and

RAMENDRA P. ROY
Department of Mechanical and Aerospace Engineering, Arizona State University, Tempe, AZ 85287, U.S.A.

(*Received* 14 *December* 1981; *in revised form* 25 *January* 1983)

Abstract—An experimental investigation of the statistical character of boiling flows has been carried out. Two flow field variables, viz. static pressure fluctuations at the test section outer wall and instantaneous chordal-average vapor fraction, were studied in vertical up-flow through concentric annular test sections. Matched piezo-electric pressure transducers were used for the pressure fluctuation measurements, and a linearized dual-beam X-ray system was used for the vapor fraction measurements. Steady state (mean) thermal-hydraulic conditions in the test section were determined by an analytical model and verified to a certain extent by capacitance probe vapor volume fraction measurements. A wide range of local conditions with flow regimes ranging from subcooled bubbly to saturated churn turbulent-slug-annular were investigated.

The wall static pressure fluctuation results include: (i) intensity (RMS value), (ii) probability density function; and (iii) autopower spectral density function. The chordal-average vapor fraction results include: (i) probability density function; and (ii) autopower spectral density function. The magnitude of coherence between wall static pressure fluctuations and chordal-average vapor fraction fluctuations are presented as well.

It is suggested that diagnosis of flow regimes on the basis of the statistical properties of the two variables studied should be possible.

1. INTRODUCTION

The inherent randomness and, in many flow regimes, the discreteness of flow field structure in boiling flows have received increased attention during recent years due to several reasons. First, it appears, on the basis of results obtained primarily from air–water cold-flow experiments (Jones & Zuber 1975; Vince & Lahey 1980), that specific statistical characteristics of local‡ vapor fraction fluctuations are uniquely dependent upon prevalent flow regimes such as bubbly, slug, annular etc. If this can be demonstrated for boiling flows as well, then regime diagnosis from either direct measurement of vapor fraction fluctuations or indirect measurement via some other system state variable strongly affected by vapor fraction fluctuations, for example, local thermal neutron flux fluctuations in boiling water nuclear reactor (BWR) cores (Thie 1963; Williams 1974; Ando *et al.* 1975; Frogner *et al.* 1976), becomes a possibility. Second, it is believed that structural vibrations induced in components in which boiling flow occurs, for example, coolant channels and fuel rods in nuclear reactor cores, tubes and shell in steam generators etc., are due primarily to static pressure fluctuations at the walls (Gorman 1971). Information regarding the intensity and spectral character of these fluctuations would therefore be of considerable value. Third, when concocting time (or ensemble) averaged, space-averaged phasic mass, momentum, and energy conservation equations for specific two-phase flow regimes from the local instantaneous equations (Ishii 1975; Delhaye & Achard 1977), one ideally

†This work was carried out when both authors were with the Nuclear Engineering Program, University of Illinois at Urbana-Champaign, Illinois, U.S.A.

‡Axially local, but usually at least chordally averaged along the transverse dimension of the channel.

should know the stochastic nature of the occurrence of each phase throughout the flow field. Correct averaging operators could possibly be defined then. Finally, it would be useful to develop a model (at least a semi-empirical one) of the process noise in boiling flow systems. Such a model, after validation by comparison with experimental findings, has several possible applications. For example, it would be possible to estimate certain transient (deterministic) characteristics of flow systems from the simulated stochastic fluctuations of pertinent state variables (such as local vapor fraction) at nominal steady state conditions (Jain & Roy 1980). Another use would be the simulation of BWR core neutron flux noise by using the boiling flow noise as an input perturbation in a reactor model.

It is clear then that fundamental understanding of the stochastic character of boiling flows can be of considerable benefit with possible wide applications in modeling, design, and operational diagnosis of many systems of engineering importance. Nevertheless, there is a lack of experimental information in this area. Some attempts have been made in recent years to measure vapor fraction fluctuations (Jones & Zuber 1975; Vince & Lahey 1981; Alekseev *et al.* 1978), wall static pressure fluctuations (Gorman 1971; Ishigai *et al.* 1965; Hubbard & Dukler 1966; Pettigrew & Gorman 1973), momentum flux fluctuations (Yih & Griffith 1970), temperature fluctuations (Alekseev *et al.* 1978), etc. in vapor–liquid flows. Except for two, (Alekseev *et al.* 1978; Pettigrew & Gorman 1973), all of these studies were conducted in adiabatic air–water flows. Furthermore, measurements in one of the two boiling flow experiments (Alekseev *et al.* 1978) were actually carried out in the unheated section of the flow channel. It is therefore likely that the results reported there would differ from measurements in diabatic boiling regions.

In this paper, we report measurements of independent and joint statistical properties of chordal-average vapor fraction fluctuations and adjacent wall static pressure fluctuations in one-component boiling flow. The measurements were performed in a vertical annular test section with heated inner wall. The X-ray beam attenuation technique was used for the measurement of vapor fraction fluctuations. Two matched piezo-electric pressure transducers were used for measuring wall static pressure fluctuations. Bubbly, churn turbulent-slug, and churn-turbulent-slug-annular flow regimes were investigated. The latter two transitional regimes were studied since it was found (from visual observations of flow structure) to be very difficult to form pure slug and annular regimes in a boiling annular channel. Statistical properties, viz., probability density function (PDF) and autopower spectral density (APSD) function, of both vapor fraction fluctuations and wall static pressure fluctuations are reported. Variation of wall static pressure fluctuation intensity with local thermal-hydraulic condition in the test section is reported. Coherence (or lack thereof) between the two fluctuating variables is presented. Finally, it is suggested that diagnosis of boiling flow regimes on the basis of the statistical characteristics of vapor fraction fluctuations and wall static pressure fluctuations should be possible.

2. THE EXPERIMENTAL FACILITY

The reported measurements were performed in an experimental loop which is shown schematically in figure 1. Refrigerant-113 was selected as the experimental fluid because its physical properties† permit high exit vapor fraction values with relatively small heating power input. Moreover, simulation of higher pressure steam–water mixture is possible at quite low operating pressure by matching liquid–vapor density ratio. A vertical test section of annular configuration consisting of an inner 304 stainless steel tube of 15.9 mm O.D. and 1.25 mm wall thickness (resistively heated to a maximum of 40 KVA) and two different outer channel assemblies were used. Each outer assembly was 38.1 mm in I.D. and consisted mainly of transparent pyrex glass pipes (to enable flow visualization) of 4.45 mm wall thickness. The first

†Boiling point: 320.75 K at 101.33 kPa; latent heat of vaporization: 146.8 kJ/kg at 101.33 kPa; thermal conductivity: 7.49×10^{-5} kJ/smK.

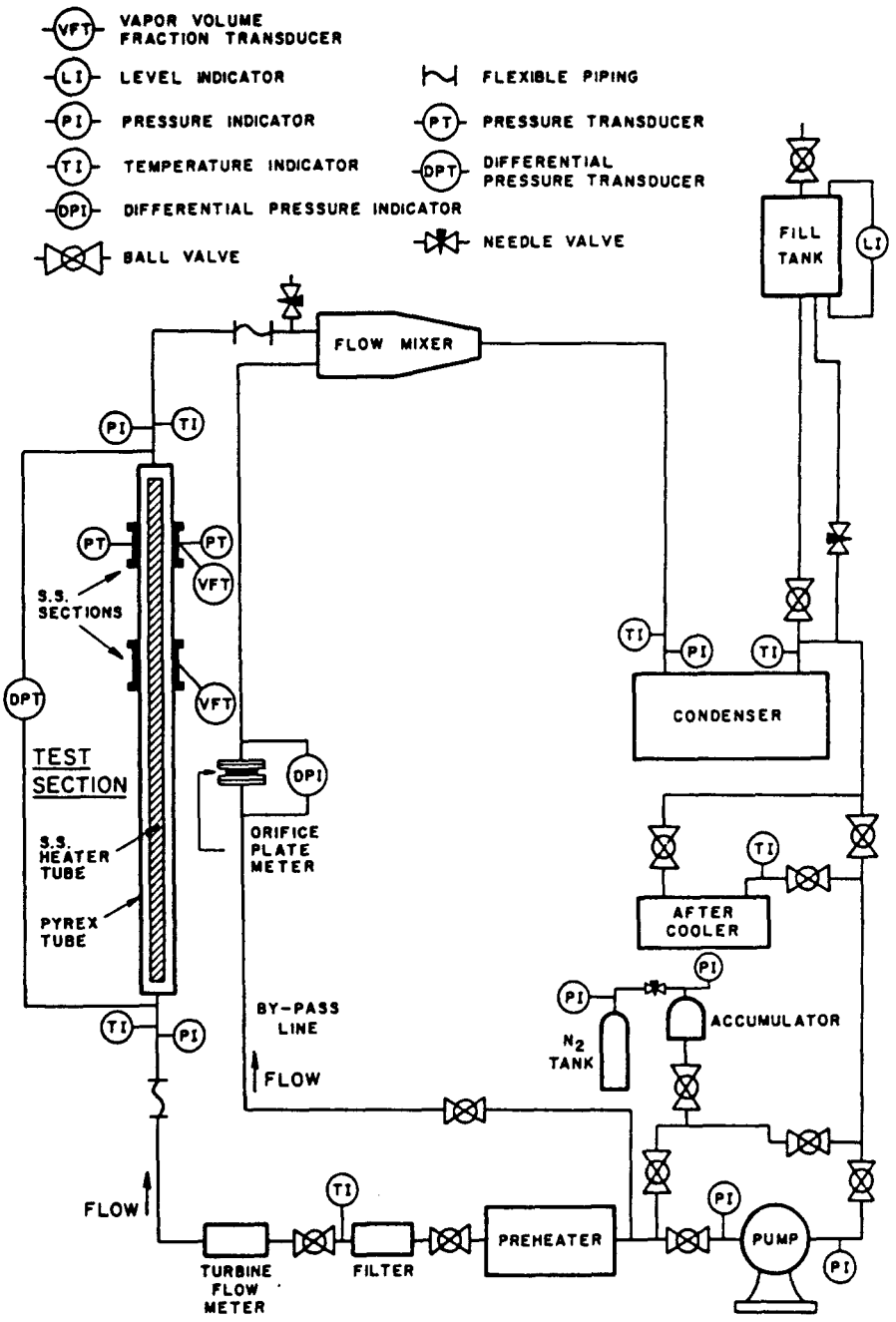

Figure 1. Schematic diagram of the experimental loop.

assembly, used for independent measurements of wall static pressure fluctuations, consisted of three pyrex pipe sections of lengths 2.438 m, 0.762 m and 0.305 m, and two 316 stainless steel sections each of wall thickness 4.45 mm and length 0.076 m, located at 2.438 m and 3.276 m,† respectively from the test section inlet. The second outer channel assembly consisted of two pyrex pipe sections of lengths 3.2 m and 0.305 m and one aluminum section‡ of 0.76 mm wall thickness and 0.152 m length, located at a distance of 3.2 m from the test section inlet. This assembly was used for all experiments involving chordal-average vapor fraction measurements. Figure 2 schematically shows the aluminum section of the second assembly. Locations of the

†This was the pressure measurement station. Each of the two stainless steel sections also served as the other electrode of the capacitance probe for mean vapor volume fraction measurements.

‡This was the measurement station.

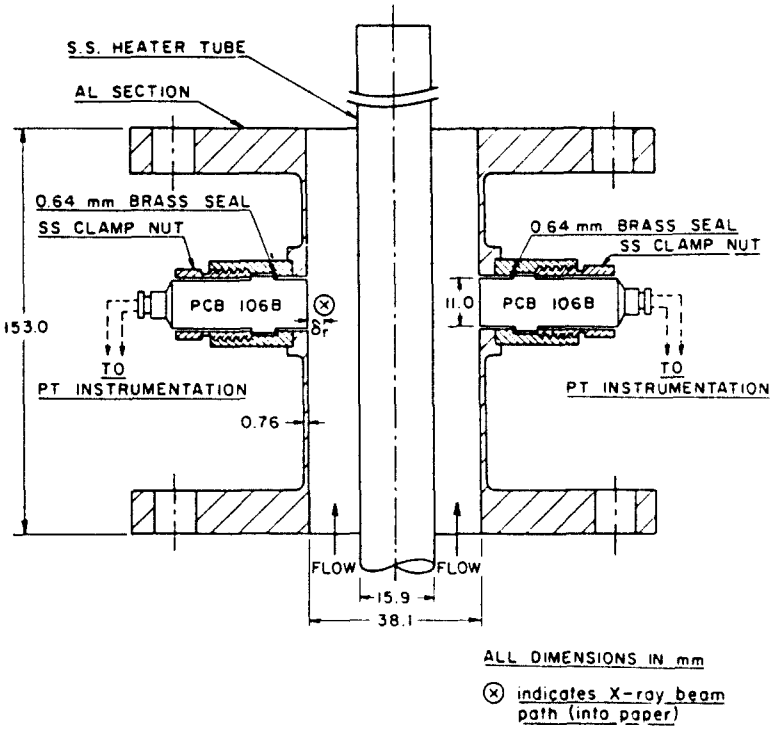

Figure 2. Schematic diagram of the measurement station.

pressure transducers for wall static pressure fluctuation measurement and orientation of the X-ray beam used for instantaneous chordal-average vapor fraction fluctuation measurements are shown.

3. THE MEASUREMENT TECHNIQUES

3.1. *Wall static pressure fluctuation measurement*

The fluctuating static pressure at any point in the flow field (including at the walls) consists of contributions from near-field sources (such as turbulence; nucleation, growth, movement and collapse of vapor bubbles; etc.) and from acoustic pressure field generated far (i.e. at least several length scales) upstream due to turbulent flow through valves, elbows, restrictions, expansions, and pump, etc. Our objective was to measure the near-field-source contribution only. However, in our test facility, not only was the far-field (extraneous) contribution found to be substantially larger than the near-field contribution, but their frequency bandwidths overlapped as well, making the extraction of information regarding the near-field contribution difficult. This necessitated the use of the "coherence technique" employing two pressure transducers with identical responses. This technique is based on the postulate that at any axial location in the test section, the far-field-source generated contribution is uniform over the flow cross-section. In accordance with this technique and as shown in figure 2, two matched, high resolution (3.046×10^{-5} V/Pa) piezoelectric pressure transducers (PCB Piezotronics, 11 mm dia. sensing surface) were installed diametically opposite to each other. Their sensing surfaces were tangential to the inner surface diameter of the measurement station (figures 2 and 8). The pressure fluctuation measurements p'_A and p'_B thus represented $p'(r_0, \theta, z_1, t)$ and $p'(r_0, \theta + \pi, z_1, t)$, respectively. The following assumptions were made in order to obtain the near-field generated pressure fluctuation information:

(i) Virtually zero hydrodynamic correlation exists between diametrically opposite locations at any axial position of an annular channel (Gorman 1971).

(ii) The flow field is statistically homogeneous over the entire flow area.

(iii) Electronic noise is negligible (for our transducers signal/noise ~ 300–400).

With these assumptions, the difference signal between the two pressure transducers p'_{AB}, can be shown to statistically represent the wall static pressure fluctuation at either A or B amplified by a factor of two. The fluctuation intensity (≡ RMS value) at the outer wall is:

$$[p'(r_o, z_1, t)]_{\mathrm{RMS}} = \left[\frac{1}{2} ACV_{p'_{AB}p'_{AB}}(\tau = 0)\right]^{1/2}. \quad [1]$$

The extent to which these measurements represent the statistical character of the static pressure fluctuations at the inner (heated) wall surface depends on the similarity of the flow fields and momentum fluctuations (especially normal to the walls) in the neighbourhood of the two walls. The measurements at the outer wall will be quite different from those at the inner wall when the bubble boundary layer at the inner wall is thin and occupies a small fraction of the wall spacing, $(r_o - r_i)$. In presence of appreciable boiling when the bubble boundary layer occupies most of the spacing, the outer wall measurements should better represent the pressure field at the inner wall. These are important considerations since the fluctuating pressure field at the heated inner wall is of considerable interest also, although far more difficult to measure directly.

3.2 *Chordal-average vapor fraction fluctuation measurement*

The X-ray beam attenuation technique was used to measure instantaneous chordal-average vapor fraction. This technique, shown schematically in figure 3, utilizes two finely collimated, identical,† mono-energetic beams of photons emitted from the same source (a dual-beam X-ray tube). The two emergent beams were measured to ensure equal intensities. One beam is passed through the test section, whereas the other one passes through a reference section of known thickness and physical properties (including X-ray absorption coefficient). The ratio of the intensity values of the beams emerging from the two sections ($I(t)$ and I_R, respectively), $R(t)$, is independent of the intensity of the incident beams. The instantaneous vapor fraction averaged over the length of the chord of the passage of the X-ray beam through the test section, $\langle\alpha\rangle_1(t)$, can be linearly related to the logarithm of this intensity ratio, $s(t)$.

$$S(t) = S_L + (S_G - S_L)\langle\alpha\rangle_1(t) \quad [2]$$

where

$$S(t) = \ln R(t) = \ln \frac{I(t)}{I_R}. \quad [3]$$

Here, S_G represents the value of $S(t)$ with the test section full of pure vapor and S_L the value of $S(t)$ with the test section full of pure liquid at a specific temperature. S_G and S_L are constant for a particular experimental setup.

The X-ray tube, a Diano Corp. model CA-8S, tungsten-target, triple-port, small-focus diffraction tube rated at 50 kV, 25 mA, was operated as a dual-beam source by sealing-off one of the three ports by a lead plate. Size of each of the two beams at the entrance location of the corresponding section was approximately 2 × 6 mm. The X-ray generator unit rated at 47 kV DC, 30 mA was a modified version of Picker Corporation Unit R2. Both the high voltage as well as the filament supply were full-wave rectified and filtered with ripple factors of less than 0.2% and 1.7% respectively at our operating conditions.

As shown in figure 3, the X-ray beams emerging from the test section and the reference section were detected by two identical detection units. Each unit consisted of an NaI(Tl) scintillation

†Same photon energy and counting statistics.

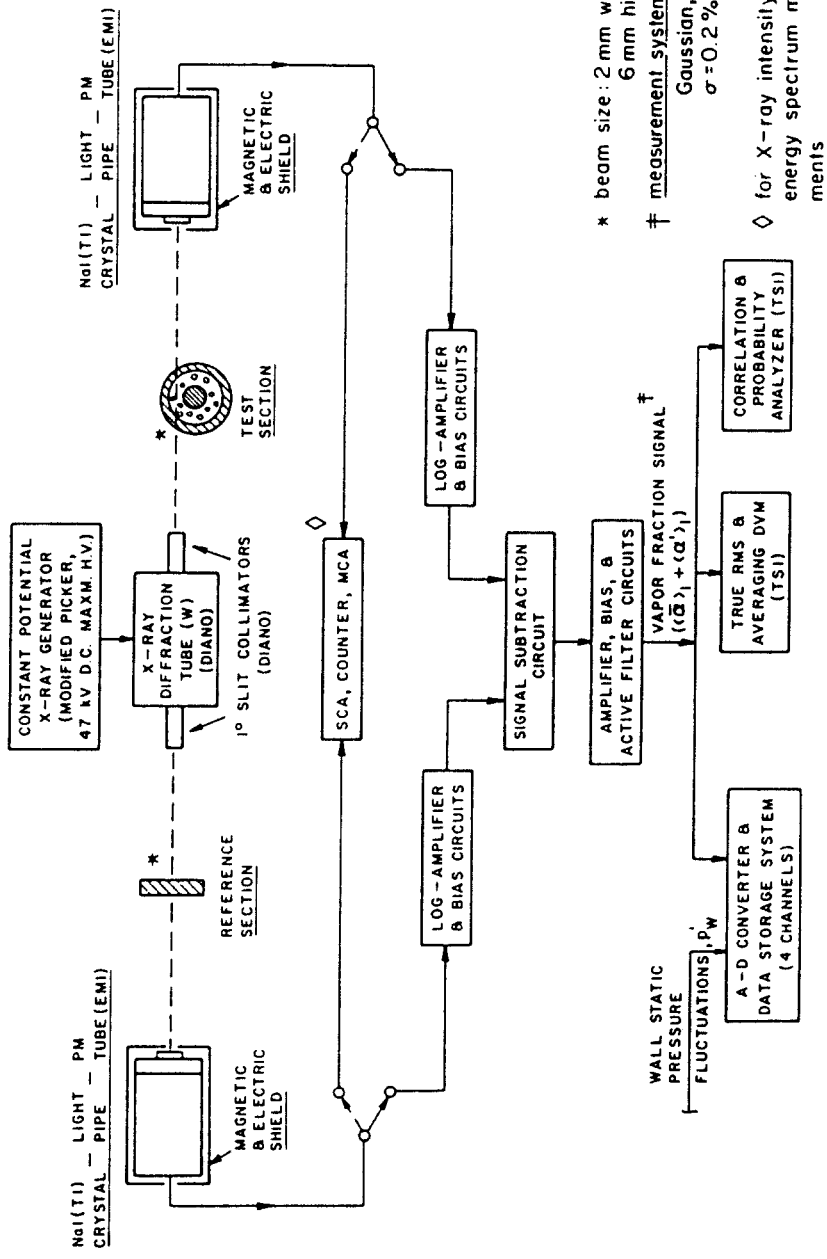

Figure 3. Schematic diagram of the dual-beam, linearized X-ray system.

crystal (Harshaw), a light pipe, and a low-noise photomultiplier tube (EMI Gencom 9635A), all assembled inside an RFI housing (EMI Gencom), which provided shielding from electric fields as well. Severe distortions of the PM tube signals were observed, in the beginning, due to the presence of excessive alternating magnetic fields associated with large heating currents (A.C.) in the test section. These distortions were reduced considerably (by a factor of over 1000) by wrapping the RFI housings in five layers of 0.25 mm thick hypernom foils (Eagle Magnetic Co.).

A single channel analyzer (SCA) and a multi-channel analyzer (MCA) were used to measure and maintain at desired level the X-ray beam intensity and its energy respectively. A typical energy spectrum with the tube operating at 40 kV and with a 4.8 mm aluminum plate filter for attenuation of lower energy X-rays is shown in figure 4.†

During all experiments reported here, the X-ray tube was operated at 40 kV and its filament current adjusted such as to maintain a count rate of 1.5×10^5 per second‡ for the beam emerging from the test section. Each of the two beams emerging from the X-ray tube were filtered through an aluminum plate filter (4.8 mm thick) before their incidence on the respective sections. The PM tubes were operated in continuous current mode for all vapor fraction measurements. Instantaneous chordal-average vapor fraction, $\langle \bar{\alpha} + \alpha' \rangle_l$, was determined as a linear function of $S(t)$ in accordance with [2] by using simple signal processing circuitry as shown schematically in figure 3. Further details can be found in Jain (1981).

Error measurements. PM tube responses to fixed test section and reference section compositions were measured to estimate the system noise§ contributions to our measurements. These contributions were found to be less than 1% for both the PM tube outputs as well as the signal $S(t)$. The fluctuations in the chordal-average vapor fraction measurement signal due to system noise only, calculated by measuring $\langle \alpha \rangle_l$-signal with pure liquid Refrigerant-113 flowing in the test section ($\langle \bar{\alpha} \rangle_l = 0.0$), were found to be Gaussian in nature (figure 5) with a standard deviation of 0.002 (0.2%) vapor fraction.

Two mock-up sections were used to establish the linearity and accuracy of the vapor fraction measurements. Ten 1.59 mm thick aluminum plates¶ comprised the first section, and four identical thin-walled (0.25 mm) aluminum troughs of such widths as to introduce 6.35 mm (per trough) of liquid Refrigerant-113 in the path of the X-ray beam when full, the second. As shown in figure 6, the maximum difference between the measured and the actual "void" fraction values was less than 2% void. The final system calibration was based on empty ($\langle \bar{\alpha} \rangle_l = 1.0$) and full-of-liquid ($\langle \bar{\alpha} \rangle_l = 0.0$) measurements in the actual test section.

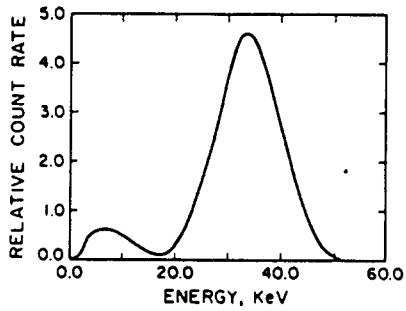

Figure 4. Typical X-ray beam energy spectrum.

†Counts obtained for energies above 40 keV were due to pulse overlapping.

‡With this count rate, the uncertainty in the measurements of vapor fraction fluctuations is less than 1% for frequencies to 20 Hz.

§System noise consists of contributions from: (i) uncertainties in the X-ray beam strength because of the statistical nature of emission from the X-ray tube target and fluctuations in the high voltage and filament excitation current; (ii) PM tube noise; and (iii) the subsequent signal-processing electronics noise.

¶The linear absorption coefficient, μ, of aluminum is close to that of liquid Refrigerant-113 in the X-ray energy range of our interest, (e.g. at 30 keV, $\mu_{Al} = 2.84\ cm^{-1}$ and, $\mu_{R\text{-}113} = 2.35\ cm^{-1}$).

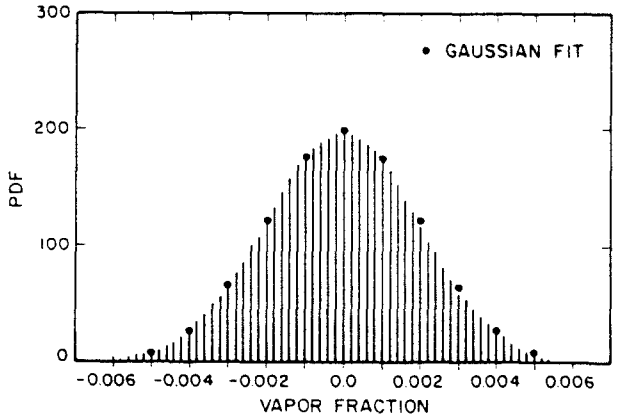

Figure 5. Probability density function of vapor fraction signal for test section full of pure liquid refrigerant-113 ($\langle\bar{\alpha}\rangle_1 = 0.0$).

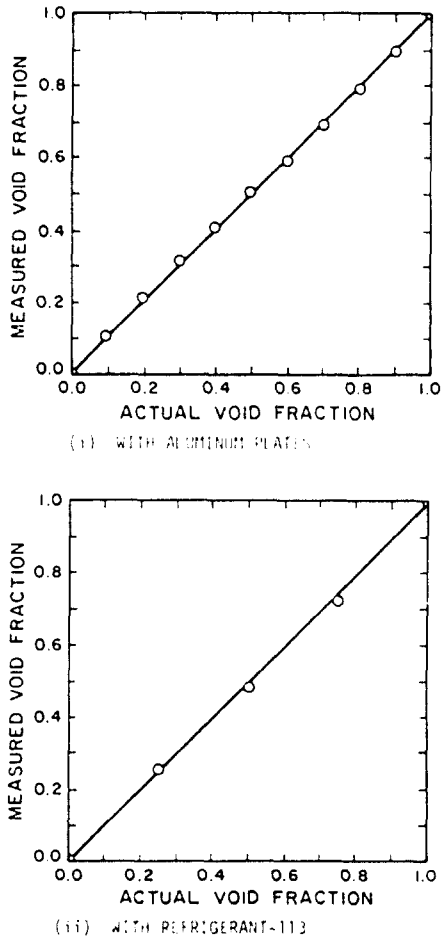

Figure 6. Linearity test of the X-ray system.

3.3 *Mean vapor volume fraction measurements*

The capacitance technique was adopted for volume-averaged mean vapor fraction measurements. Each metallic measurement station (figure 2), installed as part of the outer channel assembly, served as the outer electrode of a capacitance probe (designated VFT in figure 1), with the heater tube forming the inner electrode. A high-resolution, drift-free circuit

was constructed for the measurement of capacitance changes due to changes in local vapor volume fraction. Details of the circuit can be found in Jain (1981) and Jain *et al.* (1980). Typical measurements with the upper probe are shown in figure 10 (plotted as $\langle\bar{\alpha}\rangle_2$ vs Xeq). Analytical results obtained from an expanded version of steady state, non-equilibrium drift-flux model are also shown in the figure for comparison. The model simulated thermal-hydraulic conditions in the channel under all experimental conditions. It consisted of the cross-sectional averaged forms of the vapor continuity, mixture continuity, mixture momentum, and mixture energy conservation equations in the two-phase flow region. Appropriate correlations were used to predict axial locations of the onset of nucleate boiling (ONB) and significant net vapor generation (SNVG) points in the channel. The formulation in the single-phase liquid and subcooled boiling regions is discussed in detail in Jain *et al.* (1980) and is not presented here for brevity. As shown in figure 10, agreement between the measurements and analysis as well as the repeatability of the measurements are excellent.

3.4 *Signal analysis*

Figures 3 and 7 show schematically the signal analysis instrumentation.

Wall static pressure fluctuation intensity was measured by a true RMS meter (TSI 1060). During these measurements, active low-pass filtering of the difference signal was performed with 40 Hz upper cutoff frequency and −48 dB/octave roll-off for higher frequencies in order to reduce the 60 Hz electrical noise (this was done only after it was found that virtually all wall static pressure fluctuation energy was contained in the frequency range 0–15 Hz).

APSD functions of wall pressure and vapor fraction fluctuations were constructed by three different methods:

(i) A Correlation and Probability Analyzer (TSI 1065A) was used to construct auto-covariance function which was then Fourier transformed by a Fourier Transform Analyzer (SAI 470). Since the data storage capability of SAI 470 is rather limited (only 400 data points),

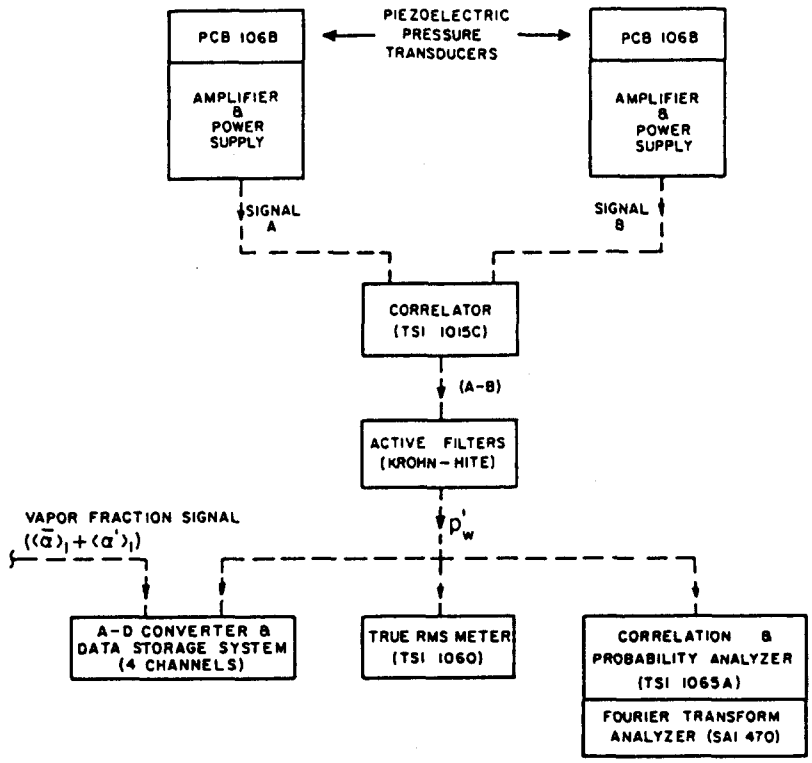

Figure 7. Pressure transducer signal analysis instrumentation.

frequency resolution of the computed APSD functions was not considered to be good enough.

(ii) Narrow frequency-band (with different center frequencies) filtering by active filters (Krohn–Hite) followed by intensity measurements by the true RMS meter—for example, true RMS value was measured at the center frequency of 0.32 Hz with lower and upper cut-off frequencies of 0.3 Hz and 0.34 Hz, respectively. Frequencies outside this narrow band were attenuated at −48 dB/octave. True RMS values were measured with the meter time constant set at 30 sec. All wall pressure fluctuation APSD functions reported in this paper were measured by this method.

(iii) Analog-to-digital conversion of the signals followed by statistical analyses of the stored data by standard digital computer techniques—for each experiment, total frequency information of each signal was divided into various frequency bands, (such as 0–1.25 Hz, 0–12.5 Hz, 0–20 Hz, etc.) due to limitations of the data acquisition system† (1024 data points in each frequency band per signal). Active filters (Krohn–Hite) were used for band-pass filtering with −24 dB/octave attenuation of the outer frequencies. Sampling interval and data acquisition duration of each time series were appropriately selected to ensure non-interference by aliasing frequencies and to satisfy ergodic hypothesis for the series. Twelve‡ experiments were conducted at each operating condition. APSD function and PDF of each signal, and coherence function between wall pressure and vapor fraction signals were constructed for each experiment. The *final* PDF, APSD function, and coherence function were then obtained by averaging the twelve individual functions. Maximum estimated statistical error in the computed magnitude of the APSD and coherence function is less than 1.8%. All the APSD functions of the chordal-average vapor fraction fluctuations, and the coherence functions reported in this paper were obtained by this method.

Probability density functions for the wall static pressure fluctuation signal and the instantaneous chordal-average vapor fraction signal were also constructed by using Correlation and Probability Analyzer. The pressure fluctuation signal was low pass filtered as in the case of other measurements with an upper cut-off frequency of 40 Hz. Three experiments were carried out at each flow boiling condition and averages of the PDFs from these experiments were computed to yield the final results. All the PDFs reported in this paper were constructed by using the Correlation and Probability Analyzer.

4. RESULTS

Experiments were conducted for the operating conditions given in table 1. Local thermal-hydraulic conditions at the measurement location were calculated by a steady state, four-equation drift-flux model referred to earlier. As stated earlier, mean vapor fraction values at the measurement stations were provided by capacitance probe measurement as well.

4.1 *Visual observation of flow regimes*

The flow regimes observed at channel locations near the measurement stations over the range of our experimental conditions could be characterized into three broad categories:

(i) *Bubbly regime.* The flow field was bubbly downstream of initiation of vapor ejection into the liquid core. Typical bubble sizes ranged from 1–2 mm dia. for low vapor fraction regions

Table 1. Range of experimental conditions

Inlet flow rate	2.72×10^{-4}–5.32×10^{-4} m³/s
Inlet pressure (absolute)	350–410 kPa
Heat flux (at inner tube surface)	1.047×10^{5}–1.31×10^{5} W/m²
Inlet subcooling	8.3–69.4 K

†APPLE II minicomputer and data acquisition system.

‡This number was optimally decided upon to obtain low statistical error, fine spectral resolution of the computed APSD functions, and adequate time series length to satisfy ergodic hypothesis in each frequency band.

(e.g. $\langle\bar{\alpha}\rangle_2 \sim 1$–3 per cent) to 4–5 mm dia. at $\langle\bar{\alpha}\rangle_2 \sim 15$–20 per cent. At high vapor fractions, froth-like (churn-turbulent) pattern formed near the outer channel, while churning bubble layers could still be seen at the heated wall proximity. At $\langle\bar{\alpha}\rangle_2 \sim 45$–50 per cent, larger vapor bubbles (typically 1–2 cm dia.) appeared with the frothy pattern still occupying the outer wall vicinity.

(ii) *Churn turbulent-slug regime.* At $\langle\bar{\alpha}\rangle_2 \sim 55$ per cent and higher, vapor slugs (elongated vapor agglomerations occupying much of the channel spacing although circumferentially occupying only a quadrant or so, figure 8), typically 2–3 cm long, existed along with churn turbulent froth-like flow in regions not occupied by the vapor slugs. The frequency at which these slugs passed the measurement station, as well as their lengths increased with increasing vapor fraction. At $\langle\bar{\alpha}\rangle_2 \sim 60$–65 per cent, approximately 4–6 cm long vapor slugs could be seen.

(iii) *Churn turbulent-slug–annular regime.* Beyond $\langle\bar{\alpha}\rangle_2 \sim 70$ per cent, an annular flow pattern could be distinguished much of the time. Here a vapor core surrounded the heater tube with churn turbulent mixture extending to the outer wall from this core interface. Occasional vapor slugs were also observed.

Over the range of experimental conditions studied it was found to be very difficult to form well-defined slug and annular regimes in the annular test section.

4.2 *Wall static pressure fluctuations*

Prior to pressure fluctuation measurements, it was deemed necessary to study the sensitivity of the piezo-electric pressure transducers to test section vibration. To this end, the same two transducers were installed at the measurement station(s) except that special mountings (one for each transducer) were installed first. Each of these mountings contained a rigidly fixed stainless steel insert which isolated the transducer sensing surface from the flowing fluid while presenting an identical surface tangential to the channel inner surface. RMS values of the transducer output signals were then measured over the entire range of experimental conditions, both in differential (A–B) mode as well as individually (A,B). Figure 9 shows typical results in equivalent Pa. The (A–B) mode yielded higher values due to the opposite orientation of the transducers with respect to the lateral movement of the test section outer channel causing parts of the responses to be added. It can be observed, by comparing figure 9 and figure 10 (to be discussed next), that only in the churn turbulent-slug–annular regime does the transducer vibration response contribute appreciably ($\simeq 14$ per cent) to the measured wall static pressure fluctuation intensity. For all other conditions, the effect of test section vibration is considerably lower.

Wall pressure fluctuation measurements were conducted initially with unheated liquid flow in the test section in an attempt to compare the measured fluctuation intensity to the ideally

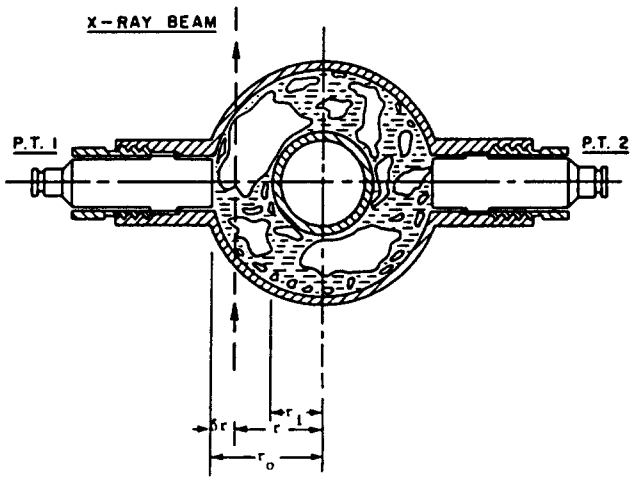

Figure 8. Churn turbulent-slug flow in the test section.

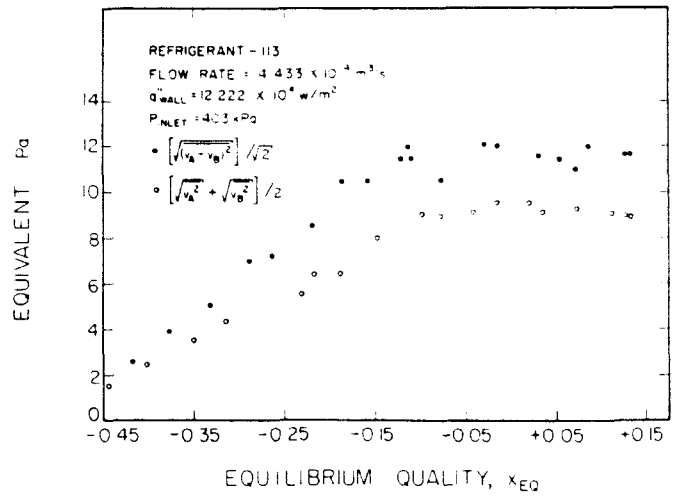

Figure 9. Sensitivity of pressure transducer to test section vibration.

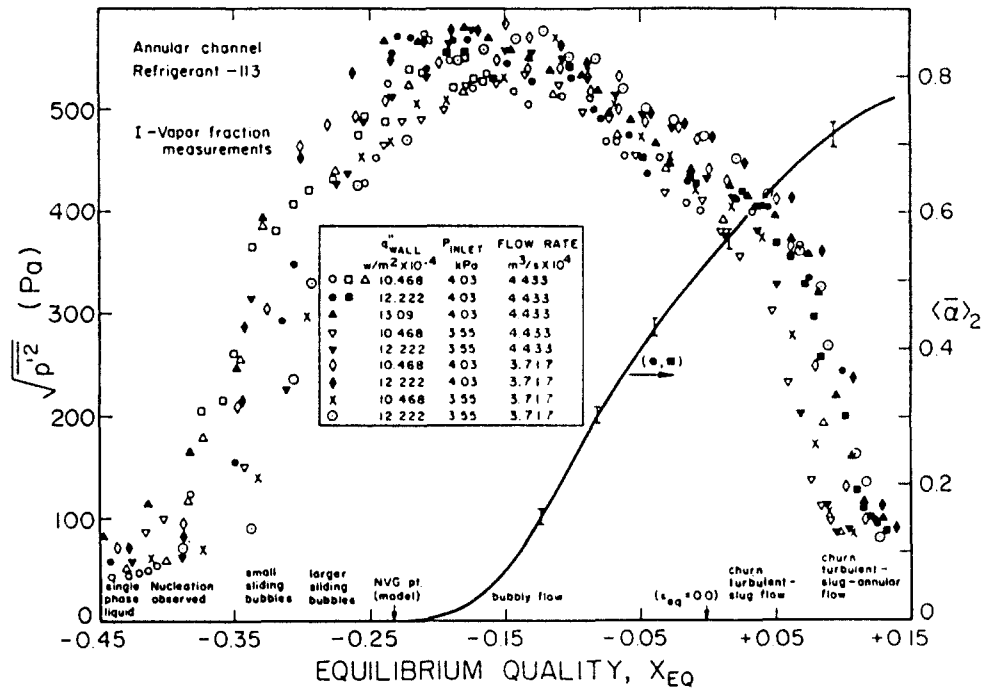

Figure 10. Variation of wall static pressure fluctuation intensity with local thermal-hydraulic condition.

expected value in hydrodynamically similar single phase flow completely free of extraneous far-field disturbances, as estimated, for example, by Wambsganss & Zaleski (1970), and Willmarth (1975). Our typical measured values (e.g. 21 Pa at liquid bulk velocity of 0.39 m/s) were usually about ten times higher than the ideal value. This indicated that we were unable to completely remove the far-field noise contamination, although a substantial improvement was clearly achieved by the use of the coherence technique.† Noting however that the wall pressure fluctuation intensity values measured in boiling flow were always considerably larger (figure 10), the error involved was considered to be acceptably small.

Figure 10 shows the static pressure fluctuation intensity measured at the outer wall as a

†Measured intensity value without using the coherence technique was 640–660 Pa at the same flow condition.

function of the calculated local (axial) bulk thermodynamic equilibrium quality. A sharp increase in intensity can be observed immediately after occurrence of vapor bubble nucleation.† This increase can be postulated to be due primarily to increased fluctuations in momentum flux normal to the wall. When dealing with single-phase liquid flow, Willmarth (1975) states that a large part of wall static pressure fluctuations is due to the interaction of velocity (momentum) fluctuations normal to the wall with the mean shear. The increasing trend in pressure fluctuation can therefore be expected to continue until the contribution from the aforementioned mechanism ceases to increase. This is probably what happens when the bubble boundary layer begins to occupy most of the flow area in the test section (e.g. at $\langle\bar{\alpha}\rangle_2 = 17$–$18$ per cent in figure 10). A further increase in the vapor fraction (with the flow regime still remaining bubbly) caused a decreasing trend in the intensity. This can be postulated to be due to a diminishing of the integrated effect, at the transducer sensing surface, of transverse momentum fluctuations as the test section gradually becomes full of vapor-liquid mixture. This decreasing trend continues until the annular flow regime is approached when a "levelling off" trend begins. Considering that in the limit of $\langle\bar{\alpha}\rangle_2 = 1.0$, the static-pressure fluctuations would once again exhibit single-phase (pure vapor flow in this case) characteristics, this leveling off of the intensity at a value somewhat higher than that for the corresponding single-phase liquid flow seems reasonable, since for the same mass flux, flow velocity would be higher for vapor flow.

Some additional comments should be made here. First, the static pressure fluctuation intensity at the inner heated wall during vapor bubble nucleation can be expected to be larger than that at the outer wall because of possible larger transverse velocity (momentum) fluctuations caused by generation, movement, and collapse of bubbles near the inner wall. The maximum intensities at the two walls should however be about the same since the pressure fields are expected to be quite similar when the bubbly mixture occupies most of the channel spacing. Second, a relatively large size of the pressure transducer sensing surface would cause some attenuation of the higher frequency fluctuations due to limited spatial resolution. Finally, the influence of boiling acoustic noise appears to be minimal for our results. This inference was arrived at by: (i) making boiling noise measurements with the same pressure transducers in a small scale no-flow setup in an anechoic chamber; and (ii) observing that the spectral content of the wall pressure fluctuations was always below ~ 15 Hz (figure 12) which is much lower than that observed for boiling acoustic noise as found by Bessho & Nishihara (1976), and Nishihara & Bessho (1977).

Figure 11 shows typical wall pressure fluctuation PDFs obtained for bubbly, churn tur-

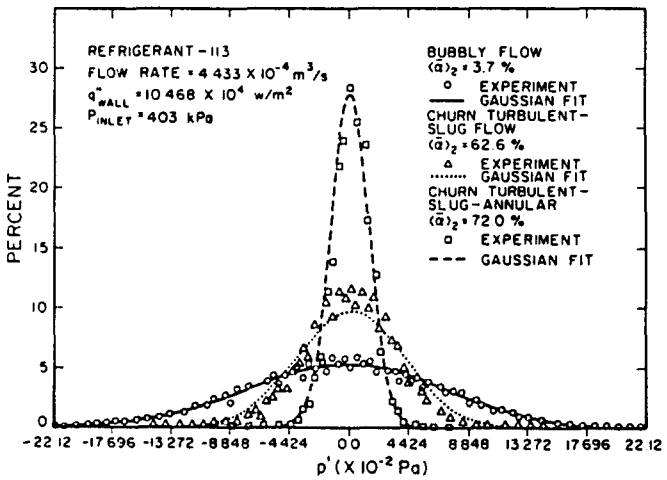

Figure 11. PDFs of wall static pressure fluctuations.

†This was usually followed immediately by bubble detachment, sliding, and occasional collapse.

bulent-slug, and churn turbulent-slug–annular flow regimes. Each PDF could be fitted reasonably well by a Gaussian distribution. The varying magnitude of the standard deviation (σ) of the Gaussian fit indicated the same variation of intensity as in figure 10. Estimates of σ were usually within 5 per cent of the intensity values shown in figure 10 for bubbly and churn turbulent-slug–annular flow regimes, and within about 12 per cent for churn turbulent-slug flow regime.

The role of flow regime as represented by spatial distribution of vapor and liquid phases in the flow field is important in determining the spectral distribution of the wall pressure fluctuations. Figure 12 depicts typical APSD functions for the three flow regimes studied. The

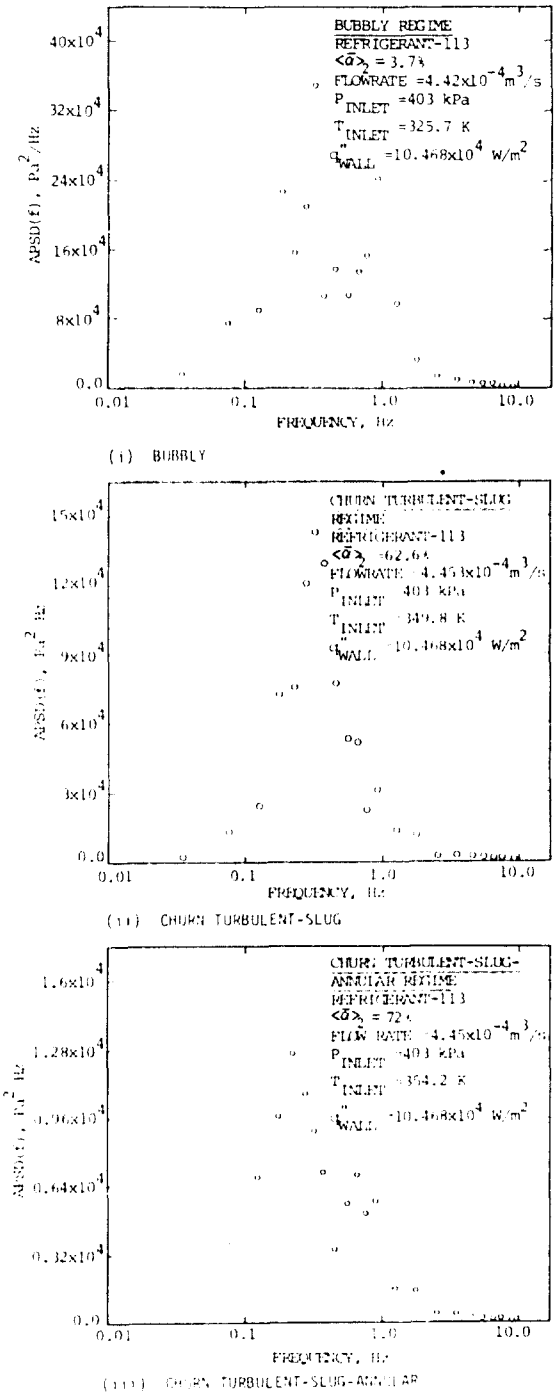

Figure 12. APSD functions of wall static pressure fluctuations in three flow regimes.

essential characteristics of these functions were invariant over the ranges of heat flux, flow rate and pressure investigated by us. Oscillograms of the corresponding pressure transducer differential signal are given in figure 13.

For all three regimes, the spectral energy is seen to be distributed primarily over the frequency band 0.03–10 Hz. The following additional characteristics can be noted:

Bubbly flow regime. Several peaks of comparable magnitudes (e.g. at 0.18 Hz, 0.32 Hz, 0.45 Hz and 0.9 Hz) are observable. Approximately 60% of the total spectral energy is contained in the frequency range 0.1–1.0 Hz. Nature of the corresponding pressure signal (figure 13(i) supports this observation.

Churn turbulent-slug flow regime. A single dominant low-frequency peak can be observed at 0.32 Hz. This peak is related to the frequency of the vapor slug passage (visually observed). Approximately 70 per cent of the total spectral energy is contained in the frequency range 0.1–1.0 Hz. Again, nature of the corresponding oscillogram (figure 13ii) supports this observation.

Churn turbulent-slug–annular flow regime. A dominant low-frequency peak (at 0.23 Hz) is observed. Total spectral energy of the signal is considerably smaller than that in the other two flow regimes. As compared to the churn turbulent-slug regime, larger relative amount of energy

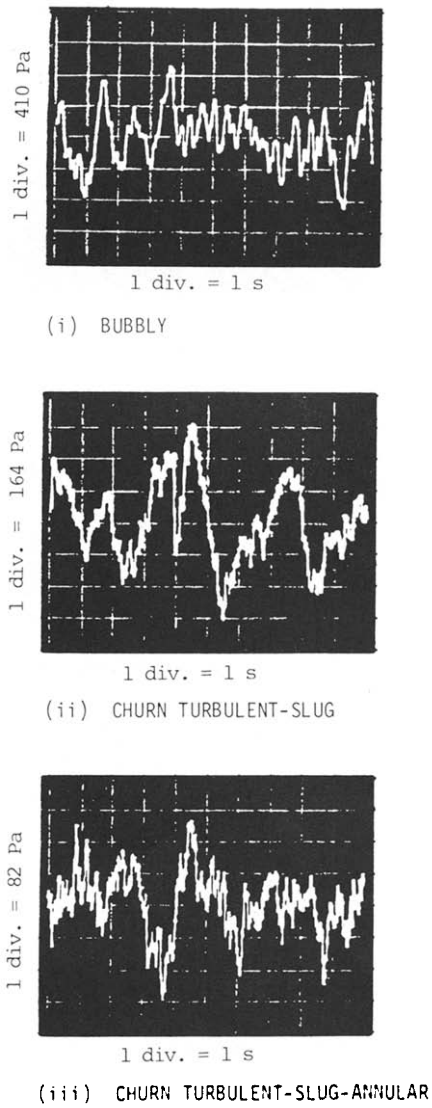

Figure 13. Oscillograms of wall static pressure signal in three flow regimes.

persists for frequencies up to 1.0 Hz. Approximately 64 per cent of the total fluctuation energy is contained in the frequency range 0.1–1.0 Hz. Nature of the corresponding oscillogram (figure 13iii) supports this observation as well.

4.3 *Chordal-average vapor fraction fluctuations*

Chordal-average vapor fraction (CAVF) measurements were conducted in the three flow regimes discussed previously. All the results presented here are for a single heat flux (1.0468×10^5 W/m^2 at the inner wall), and inlet pressure (365 kPa absolute) but different flow rates (ranging from 2.967×10^{-4} m^3/s to 5.317×10^{-4} m^3/s). The various thermal-hydraulic conditions at the measurement station were created by altering the test section inlet subcooling. Three oscillograms of the CAVF signal, one for each flow regime, are shown in figure 14(i)–(iii).

Use of PDFs has been suggested for diagnosis of flow regimes in air–water flows, by Jones & Zuber (1975), and Vince & Lahey (1981). In a similar attempt here, PDFs of instantaneous CAVF were constructed for the three flow regimes. Typical ones obtained are shown in figures 15–17. Nominal flow conditions, local area-averaged mean vapor fraction and calculated values†

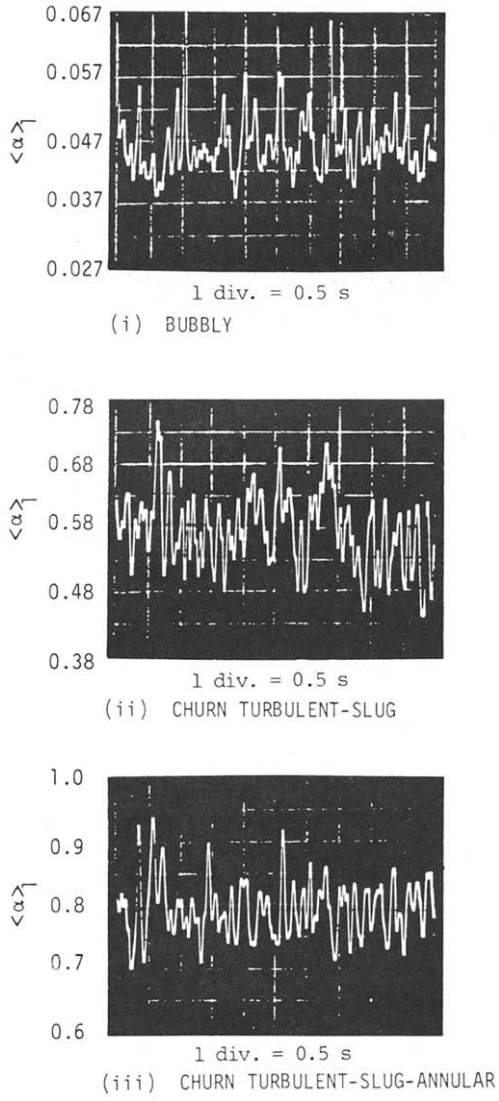

Figure 14. Oscillograms of chordal-average vapor fraction fluctuation in three flow regimes.

†Values calculated by the steady-state four-equation drift flux model.

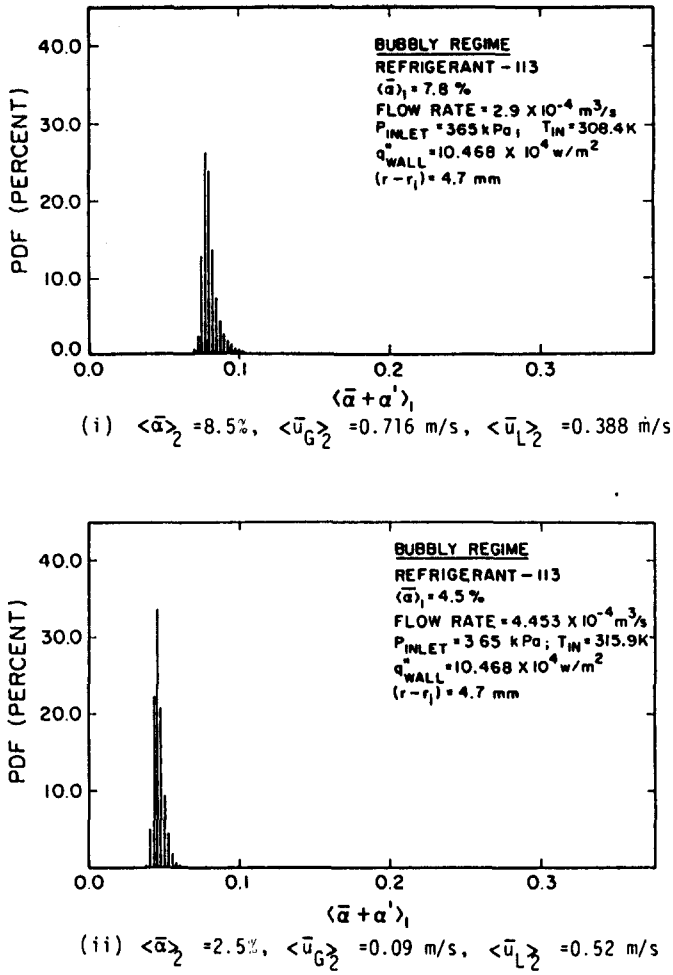

Figure 15. PDFs of chordal-average vapor fraction in bubbly flow for two different flow rates.

of vapor and liquid velocities at the channel axial location of measurement are listed on each figure. Some important characteristics of the PDFs are:

Bubbly flow regime. A single, narrow-peaked distribution occurs in the low vapor fraction region for each of the two cases shown (figure 15i, ii). The small width of the distribution suggests the presence of a relatively homogeneous flow field (from vapor bubble size and spatial distribution considerations) in time domain for this flow regime. This was confirmed by our visual observations as well. The discernible tail on the high vapor fraction side of each PDF is possibly due to occasional passage of larger bubbles. This is also indicated by the occasional sharp peaks in the oscillogram of figure 14(i).

Churn turbulent-slug flow regime. A single, wide-peaked distribution can be seen for each of the two cases shown (figure 16i, ii). The larger width of the distribution suggests the presence of a heterogeneous flow field (in terms of vapor agglomeration size and spatial distribution) in the time domain. The twin-peaked distribution reported for measurements in well-defined slug flow in air–water experiments by Jones & Zuber (1975), and Vince & Lahey (1980) could not be obtained here because of the presence of relatively high vapor fraction churn turbulent fluid in between the vapor slugs in place of very low vapor fraction fluid (a few air bubbles in water) in air–water experiments. One can however notice a slight "hump" at $\langle\alpha\rangle_l \sim 0.5$ for each case. This feature, none-too-significant statistically, could be due to the churn turbulent part of the flow, with the higher vapor fraction peak reflecting the passage of vapor slugs.

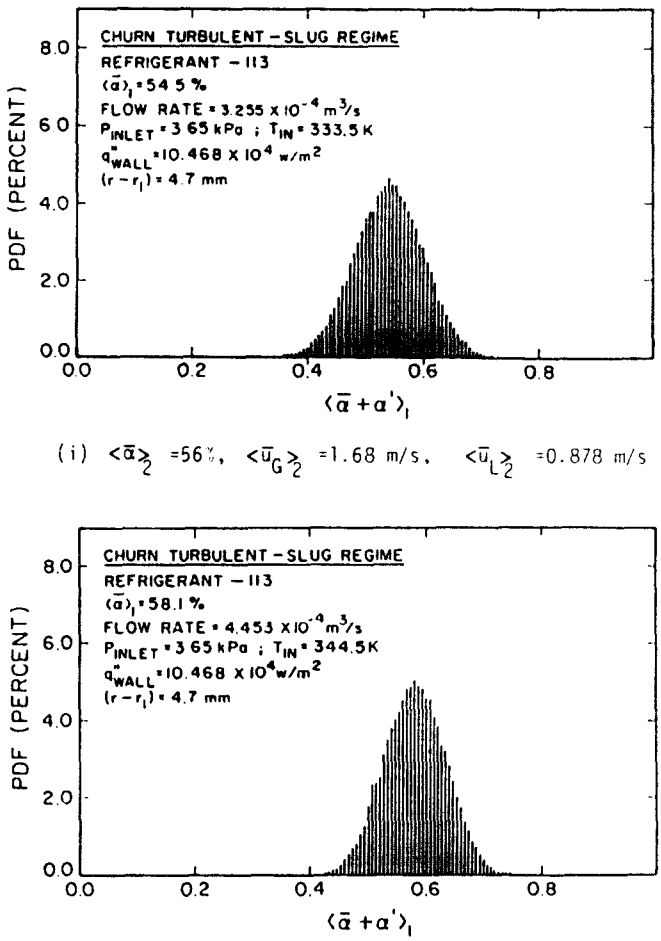

Figure 16. PDFs of chordal-average vapor fraction in churn turbulent-slug flow for two different flow rates.

Churn turbulent-slug–annular flow regime. Each of the two PDFs shown in figure 17 has single peaked distribution in the high vapor fraction region. The distribution is much narrower in comparison to that obtained for the churn turbulent-slug regime. Occasional passage of vapor slugs accompanied by churning vapor–liquid mixture is indicated by a small tail on the low vapor fraction side of the PDF.

Typical APSD functions computed from the CAVF fluctuation measurements in the three flow regimes are presented in figures 18–20. Most of the spectral energy can be seen to be contained in the frequency range 0.01–15.0 Hz for all cases. The following characteristics can also be noted:

Bubbly flow regime. Figure 18 shows three APSD functions obtained for three different flow conditions. These are seen to have very similar features. Several comparable peaks can be observed in the frequency range 0.05–1.0 Hz. The APSD function magnitude drops off monotonically for frequencies higher than 1 Hz.

Churn turbulent-slug flow regime. The APSD functions obtained for three different flow conditions are shown in figure 19. Again, the three functions have very similar characteristics. For the two higher flow rate cases (figure ii, iii), strong low-frequency peaks corresponding to the respective frequencies of vapor slug passage at the measurement station (as observed visually) can be seen. Recall that the same feature was observed for wall pressure fluctuations in this flow regime (figure 12ii). For the low flow rate case (figure 19i), the peak is not quite as well-defined but spread over 0.05–0.5 Hz range indicating that the vapor slugs are passing

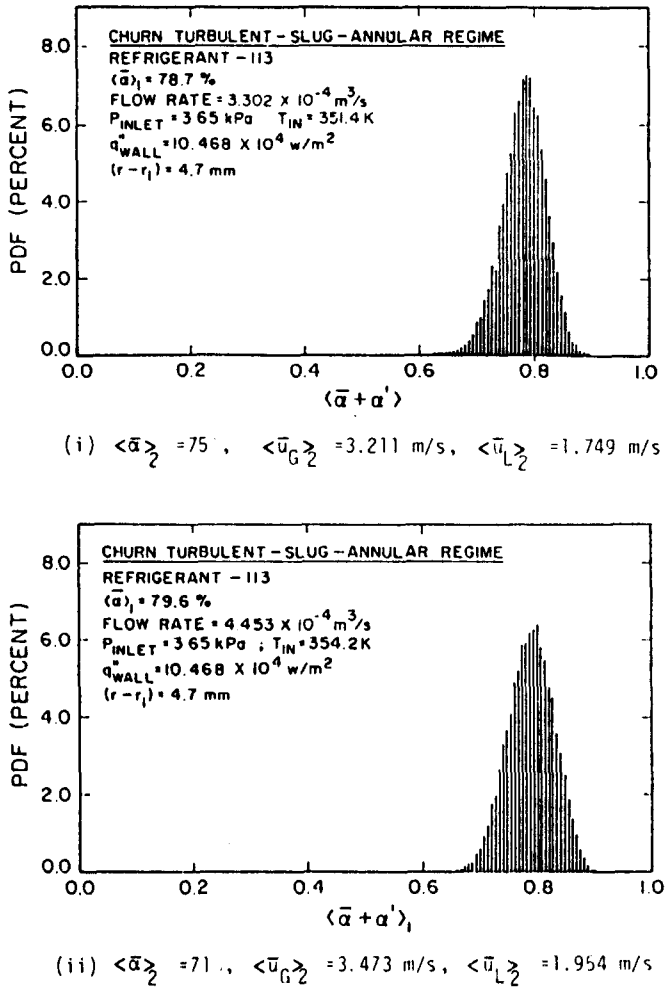

Figure 17. PDFs of chordal-average vapor fraction in churn turbulent-slug-annular flow for two different flow rates.

somewhat non-periodically here. All three APSD functions have appreciable magnitudes for frequencies up to 6 Hz, beyond which they drop off sharply.

Churn turbulent-slug-annular flow regime. The APSD functions, shown in figure 20 for three different flow conditions, exhibit a definite shift of CAVF fluctuation energy toward higher frequencies in comparison to the other two flow regimes. In each case a flow rate-dependent dominant frequency (larger than 1 Hz) exists. This is possibly due to disturbance waves of specific (depending on vapor and liquid flow rates) wavelengths at the interface between vapor core and frothy mixture during the annular part of the flow. Surprisingly, no peak appears at low frequency corresponding to vapor slug passage (see figure 12iii for such a peak in the wall static pressure fluctuation APSD function). Furthermore, no similar shift of energy to higher frequencies can be seen in the outer wall pressure fluctuation APSD function. This could be due to severe attenuation, by the intervening frothy mixture, of the pressure perturbations induced by the interfacial waves. The lack of low frequency peak in the CAVF APSD function is probably because of the relatively low amount of fluctuation energy contained in the slug-passage part of the flow (compared to the interfacial wave part).

The total fluctuation energy (= variance) was consistently found to be the smallest for bubbly regime and the largest for churn turbulent-slug regime and of intermediate value for the churn turbulent-slug-annular regime. This trend was invariant with respect to the nominal flow conditions. One may conclude that flow heterogeneity (in terms of vapor agglomeration size and

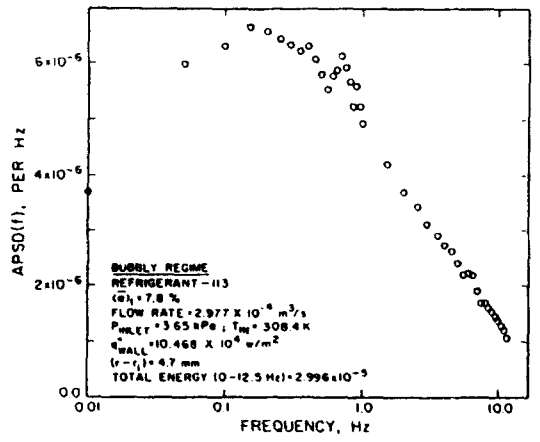

(i) $\langle \bar{\alpha} \rangle_z$ =8.5%, $\langle \bar{u}_G \rangle_z$ =0.716 m/s, $\langle \bar{u}_L \rangle_z$ =0.388 m/s

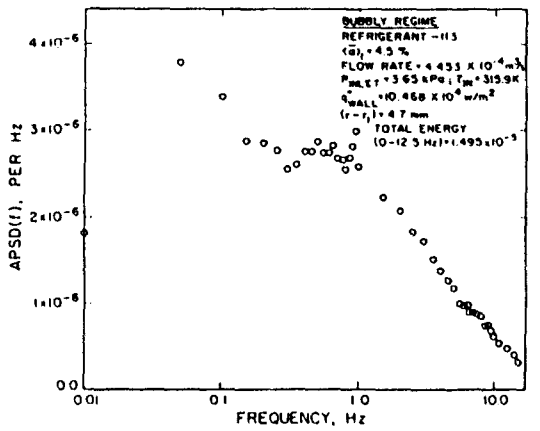

(ii) $\langle \bar{\alpha} \rangle_z$ =2.5%, $\langle \bar{u}_G \rangle_z$ =0.09 m/s, $\langle \bar{u}_L \rangle_z$ =0.52 m/s

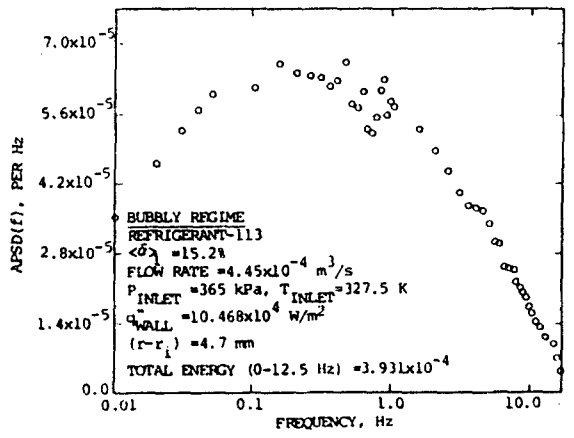

(iii) $\langle \bar{\alpha} \rangle_z$ =14.5%, $\langle \bar{u}_G \rangle_z$ =0.92 m/s, $\langle \bar{u}_G \rangle_z$ =0.56 m/s

Figure 18. APSD functions of chordal-average vapor fraction fluctuations in bubbly flow for three different flow conditions.

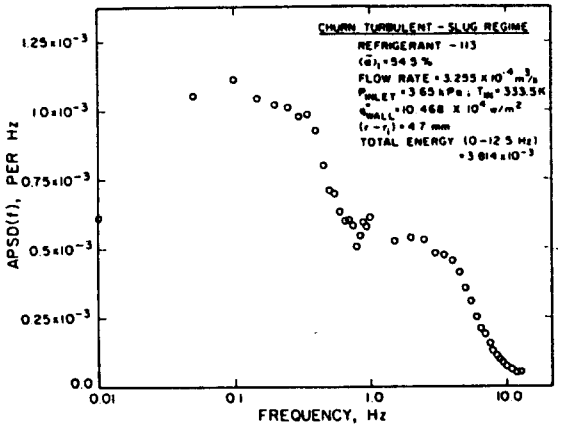

(i) $\langle \bar{\alpha} \rangle_2$ =56%, $\langle \bar{u}_G \rangle_2$ =1.68 m/s, $\langle \bar{u}_L \rangle_2$ =0.878 m/s

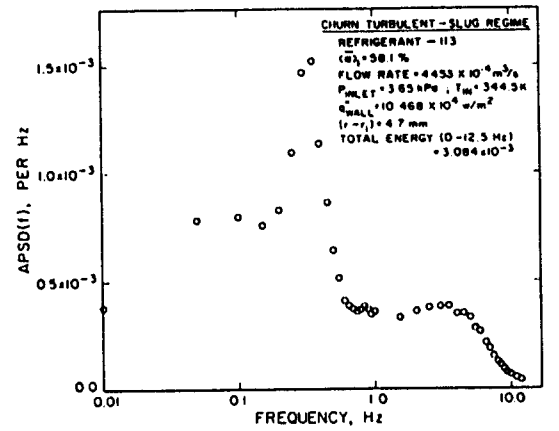

(ii) $\langle \bar{\alpha} \rangle_2$ =57%, $\langle \bar{u}_G \rangle_2$ =2.21 m/s, $\langle \bar{u}_L \rangle_2$ =1.202 m/s

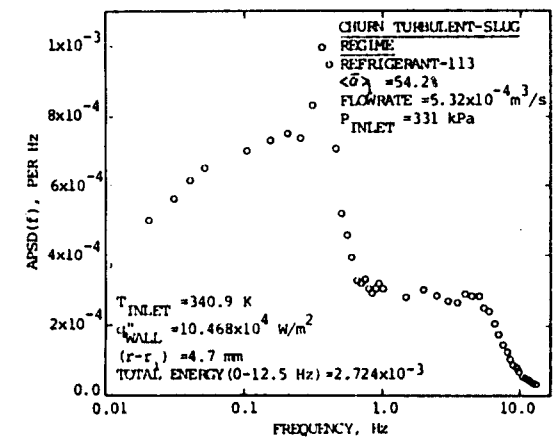

(iii) $\langle \bar{\alpha} \rangle_2$ =53.9%, $\langle \bar{u}_G \rangle_2$ =2.258 m/s, $\langle \bar{u}_L \rangle_2$ =1.286 m/s

Figure 19. APSD functions of chordal-average vapor fraction fluctuations in churn turbulent-slug flow for three different flow conditions.

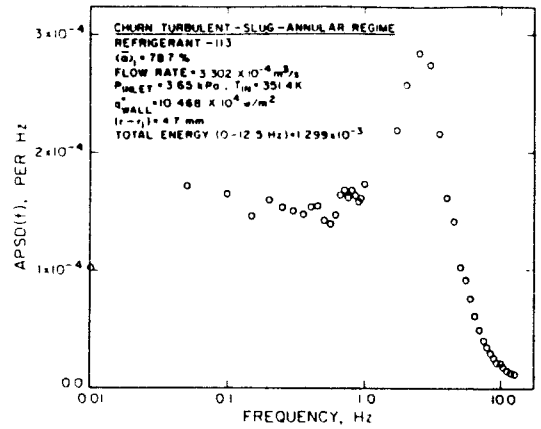

(i) $\langle \bar{\alpha} \rangle_2 = 75$, $\langle \bar{u}_G \rangle_2 = 3.211$ m/s, $\langle \bar{u}_L \rangle_2 = 1.249$ m/s

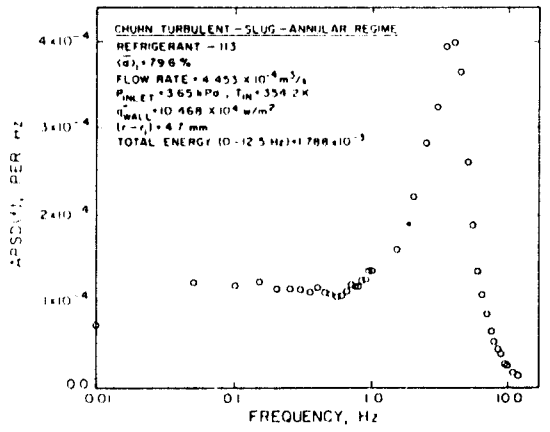

(ii) $\langle \bar{\alpha} \rangle_2 = 71$, $\langle \bar{u}_G \rangle_2 = 3.473$ m/s, $\langle \bar{u}_L \rangle_2 = 1.954$ m/s

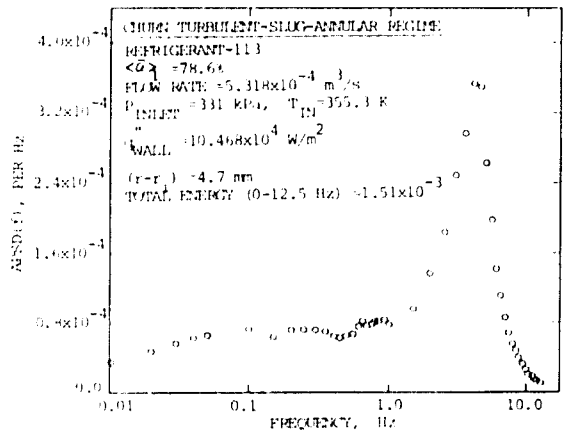

(iii) $\langle \bar{\alpha} \rangle_2 = 74.1$, $\langle \bar{u}_G \rangle_2 = 5.016$ m/s, $\langle \bar{u}_L \rangle_2 = 2.489$ m/s

Figure 20. APSD functions of chordal-average vapor fraction fluctuations in churn turbulent-slug-annular flow for three different flow conditions.

spatial distribution) in the time domain was maximum for the churn turbulent-slug regime, minimum for bubbly and in-between these for churn turbulent-slug–annular. The same conclusions can be derived from the instantaneous CAVF PDF also.

It is interesting to note that a qualitatively similar shift of fluctuation energy towards higher frequencies with increasing local mean vapor fraction and consequent changes in flow regime have been observed by Ando *et al.* (1975) and Frogner *et al.* (1976), in thermal neutron flux fluctuation data obtained from BWRs. The main cause was hypothesized by these authors to be fluctuations in the local vapor fraction of the coolant (steam–water mixture). The spectral distribution results presented in this paper appear to lend credence to this hypothesis. In an effort to quantify the spectral shift in fluctuation energy, we calculated the energy fraction ratio:

$$\frac{\text{CAVF fluctuation energy in the frequency band 2–6 Hz}}{\text{Total CAVF fluctuation energy}}.$$

Figure 21 is a plot of this ratio against the local mean chordal-average vapor fraction.

As noted earlier, strong periodicities appear in the CAVF fluctuations for the churn turbulent-slug and churn turbulent-slug–annular flow regimes. The dominant frequency (defined as the frequency at which a distinct maximum in the APSD function occurs) appears to be dependent on the local mixture volumetric flow rate. Figure 22 shows a plot of dominant frequency vs local volumetric flow rate for the two flow regimes.

4.4 *Coherence between wall static pressure fluctuations and adjacent region vapor fraction fluctuations*

Coherence between static pressure fluctuations at the outer wall and adjacent region vapor fraction fluctuations (as represented by CAVF measurements) was computed for different

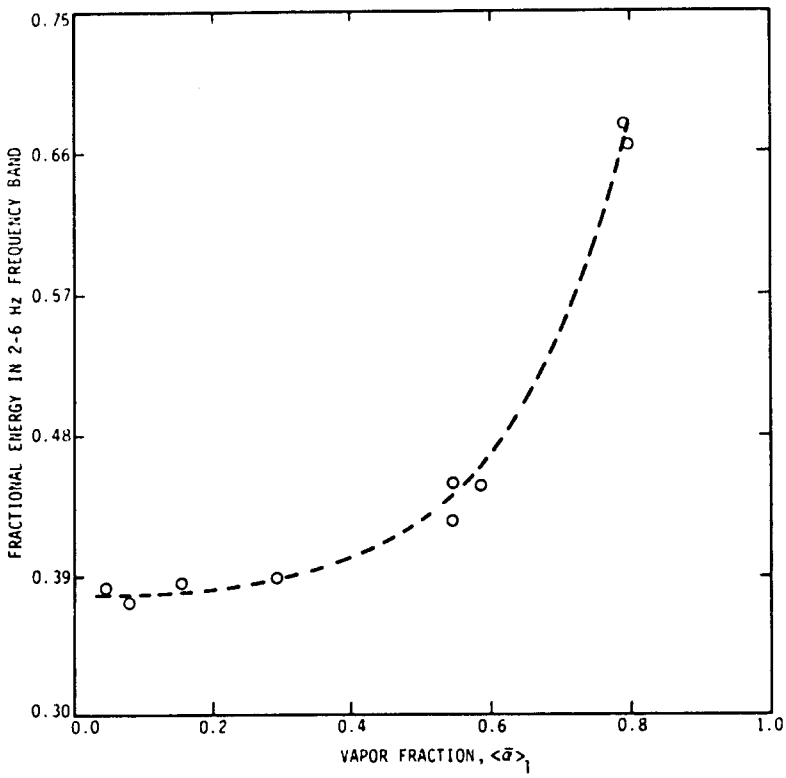

Figure 21. Variation of fraction of the total spectral energy in 2–6 Hz frequency band with mean chordal-average vapor fraction.

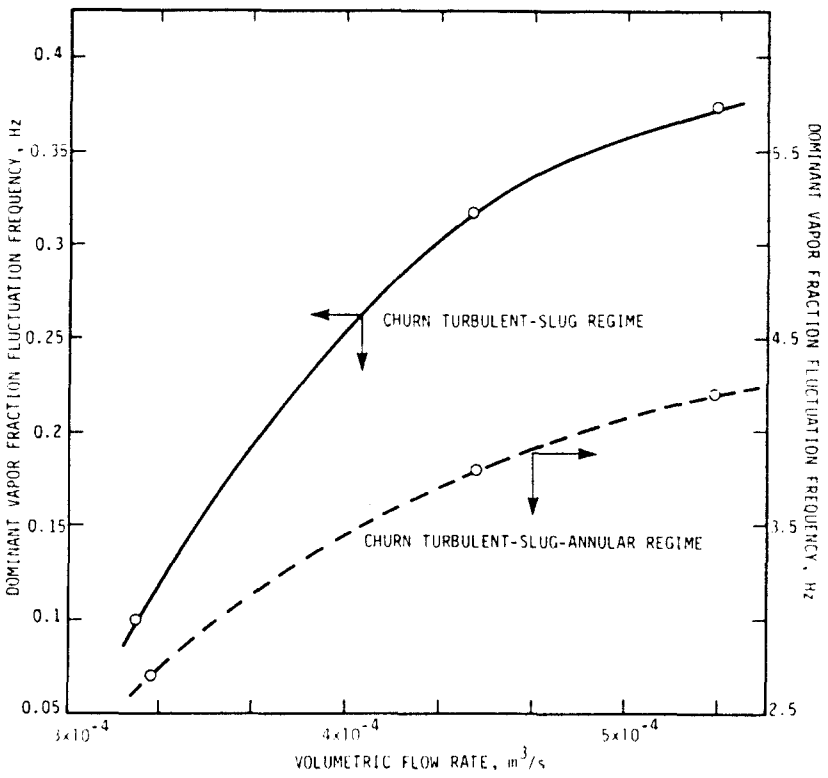

Figure 22. Variation of dominant frequency determined from APSD functions of vapor fraction fluctuations with local volumetric flux.

values of the radial separation between pressure transducer sensing surface and the X-ray beam location (δr, figure 2) for the three flow regimes. Typical coherence functions obtained for $\delta r = 6.4$ mm are shown in figure 23(i)–(iii). Some notable features are:

Bubbly flow regime. The coherence function indicates a none-too-strong correlation between the wall pressure fluctuations and the CAVF fluctuations. However, if CAVF fluctuations only in the vicinity of the pressure transducer sensing surface (as opposed to the whole chord) could be measured and used to calculate the coherence, its magnitude would have been somewhat higher (perhaps by as much as 60–70 per cent of the present value).† Measurements with smaller δr (for example, 4.8 mm) show a small increase in the coherence function magnitude with decreasing δr. It appears reasonable to postulate that a part of the wall static pressure fluctuations in bubbly flow is caused by the vapor fraction fluctuations in adjacent region.

Churn turbulent-slug regime. A strong peak, similar to those observed in APSD functions of both wall pressure fluctuations and CAVF fluctuations can be seen at 0.35 Hz in figure 23(ii). This strengthens our earlier contention that a strong correlation exists between the passage of vapor slugs and the wall pressure fluctuations in this regime.

Churn turbulent-slug–annular regime. The coherence is seen to be rather weak for $\delta r =$ 6.4 mm (figure 23(iii)). Regults for $\delta r = 4.8$ mm were about the same. As noted earlier, the effect of the interfacial waves as felt by the outer wall probably becomes considerably dampened due to the presence of frothy mixture in-between.

5. KEY OBSERVATIONS AND CONCLUDING REMARKS

The results reported here on the stochastic character of one-component boiling flow pertain to the bubbly flow regime and two higher vapor fraction transitional regimes, viz. churn

†This estimate is based on X-ray beam dimensions, chord length, and pressure transducer sensing surface dimensions.

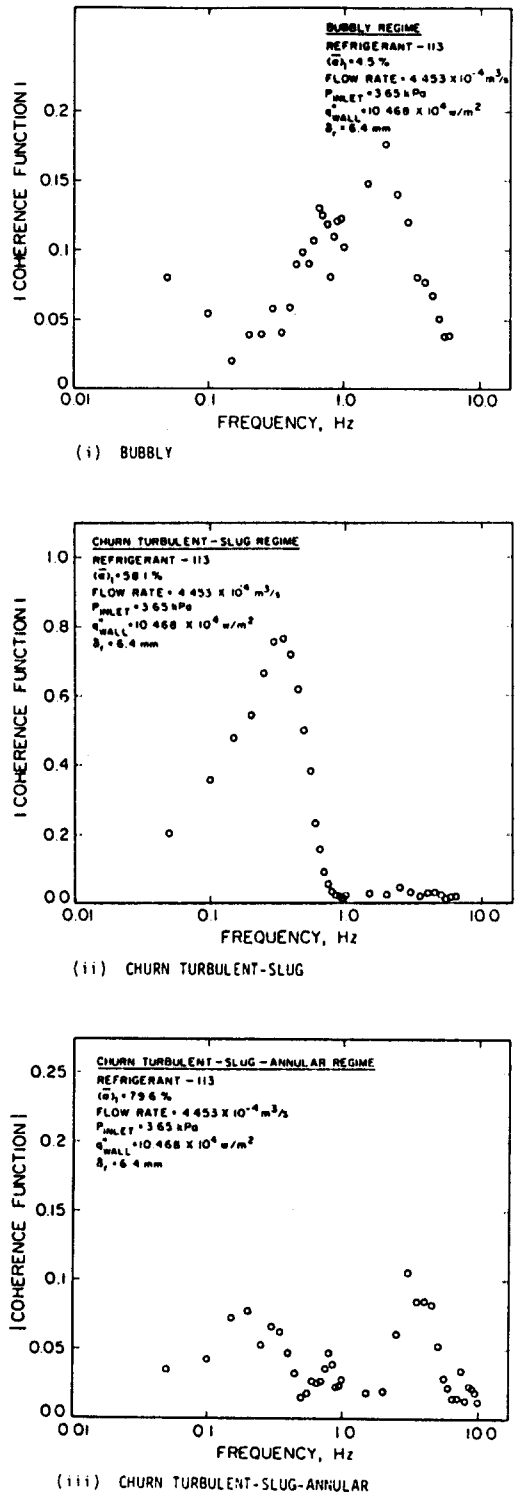

Figure 23. Coherence between chordal-average vapor fraction fluctuations and wall static pressure fluctuations in the three flow regimes.

turbulent-slug regime and churn turbulent-slug–annular regime. It should be possible to establish a more well defined form of annular regime in tubular channels, although at the expense of flow visualization. The following are our key observations:

(1) Wall static pressure fluctuations are approximately Gaussian in nature in boiling flow. Their intensity exhibits a consistent trend with local thermal-hydraulic condition, reaching a maximum in bubbly regime when the vapor fraction is sufficiently high to cause the channel flow area to be fully occupied by the bubbly mixture. A slowly diminishing trend in intensity begins as the flow approaches slug condition and continues through the churn turbulent-slug–annular regime. As the local mean cross-sectional average vapor fraction reaches high values (for example, greater than 80 per cent), an asymptotic decrease towards the expected intensity value corresponding to pure vapor flow at the prevailing mass flow rate occurs.

The extent of coherence between wall pressure fluctuations and vapor fraction fluctuations in adjacent region indicates that at least a part of the pressure fluctuations is due to the passage (random, or quasi-periodic, depending on the local flow regime) of vapor bubbles, slugs etc. at close proximity to the wall.

(2) Spectral distribution of wall static pressure fluctuation energy exhibits a clear dependence on the local flow regime. In all cases, almost all of the fluctuation energy is contained within the range 0.03–10 Hz, the major fraction being within 0.05–2.0 Hz. For both bubbly and churn turbulent-slug–annular regimes, comparable energy level is maintained through the frequency range 0.03–1 Hz. A single dominant peak at a frequency related to the passage of vapor slugs appears in the APSD function for the churn turbulent-slug regime.

(3) Probability density functions of instantaneous chordal-average vapor fraction for bubbly and churn turbulent-slug–annular regimes exhibit single peaked distributions at low and high mean vapor fraction values, respectively. The peak is considerably narrower in the case of bubbly regime indicating a more homogeneous flow structure locally, in time domain. Probability density function for churn turbulent-slug regime exhibits a single wide-peaked distribution, with a noticeable "hump" on the low vapor fraction side. The latter feature is postulated to be due to the churn turbulent part of the flow.

(4) Almost all of the vapor fraction fluctuation energy is contained in the frequency range 0–15 Hz for the flow conditions studied. For the same mass flux, there are distinct differences between the spectral distributions of this energy for the three flow regimes investigated. In bubbly regime, the fluctuation energy has comparable values at several frequencies in the range 0.1–1 Hz. Either one dominant frequency or a dominant frequency band emerges in the cases of churn turbulent-slug and churn turbulent-slug–annular regimes. The value of the dominant frequency or frequency band appears to be dependent upon the local volumetric flux.

(5) The total chordal-average vapor fraction fluctuation energy depends upon the local flow regime. Its value was consistently found to be the smallest for bubbly regime and the largest for churn turbulent-slug regime. The value was of intermediate magnitude but of the same order as churn turbulent-slug for the churn turbulent-slug–annular regime. A gradual shift of this energy towards higher frequencies was noticeable with increasing local mean vapor fraction.

(6) Objective diagnosis of boiling flow regimes on the basis of probability density function, auto power spectral density function, and intensity (≡ RMS value) of chordal-average vapor fraction fluctuations and wall static pressure fluctuations should be possible.

(7) Further experimental work, in various boiling flow regimes, on the stochastic local occurrence of vapor and liquid phases is necessary in order that correct scales for time- and space-averaging operators may be concocted.

Acknowledgement—This research was partially funded by National Science Foundation (Heat Transfer Program) grants ENG-7706680 and CME-7920166. Parts of this paper appeared separately in two AICHE Symposium Series Nos. 199 (Vol. 76, 1980) and 208 (Vol. 77, 1981).

REFERENCES

ALEKSEEV, G. V., IBRAGIMOV, M. G., NEVSTRUEVA, E. D., RYABTSEN, V. A., SABELEV, G. D. & TYUTYAEV, V. V. 1978 Some spectral characteristics of two-phase non-equilibrium flows. *Proc. 6th Int. Heat Transfer Conf., Toronto, Canada*, Paper FB-11.

ANDO, Y., NAITO, N., TANAKE, A. & KITAMURA, N. 1975 Void detection in BWR by noise analysis. *J. Nucl. Sci. Technol.* **12**, 597–599.

BESSHO, Y. & NISHIHARA, H. 1976 Boiling acoustic emission and bubble dynamics in nucleate boiling. *J. Nucl. Sci. Technol.* **13**, 520–522.

DELHAYE, J. M. & ACHARD, J. L. 1977 On the use of averaging operators in two-phase flow modeling. *Thermal Hyd. Aspects Nucl. Reactor Safety (ASME)* **1**, 289–332.

FROGNER, B., ROY, R. P. & CARMICHAEL, L. A. 1976 Relations between void and LPRM noise in BWRs. *Trans. Am. Nucl. Soc.* **24**, 415–416.

GORMAN, D. J. 1971 An analytical and experimental investigation of the vibration of cylindrical reactor fuel elements in two-phase parallel flow. *Nucl. Sci. Engng* **44**, 277–290.

HUBBARD, M. J. & DUKLER, A. E. 1966 The characteristics of flow regimes for horizontal, two-phase flow. *Proc. Heat Transfer and Fluid Mechanics Institute*, University of Santa Clara.

ISHIGAI, S., YAMANE, M. & ROKO, K. 1965 Measurement of the component flows in a vertical two-phase flow by making use of the pressure fluctuations. (Part 1, Proposal of a characteristic number). *Bull. JSME* **8**, 375–382.

ISHIGAI, S., YAMANE, M., ROKO, K., TAKAGI, T. & TANAKA, K. 1965 Measurement of the component flows in a vertical two-phase flow by making use of the pressure fluctuations. (Part 2, The flow model for slug-flow and its application). *Bull. JSME* **8**, 383–390.

ISHII, M. 1975 *Thermo Fluid Dynamic Theory of Two-phase Flow.* Eyrolles, Paris.

JAIN, P. K. 1981 On the statistical nature of boiling flows—an experimental approach. Ph.D. Thesis, Nuclear Engineering Program, University of Illinois at Urbana-Champaign.

JAIN, P. K., NOURMOHAMMADI, K. & ROY, R. P. 1980 A study of forced convective subcooled boiling in heated annular channels. *Nucl. Engng Design*, **60**, 401–411.

JAIN, P. K. & ROY, R. P. 1980 Estimation of transient responses by spectral analysis of simulated stochastic vapor fraction fluctuations in boiling flow. *Numer. Heat Transfer* **3**, 381–390.

JONES JR., O. C. & ZUBER, N. 1975 The interrelation between void fraction fluctuations and flow patterns in two-phase flow. *Int. J. Multiphase Flow* **2**, 273–306.

NISHIHARA, H. & BESSHO, Y. 1977 Acoustic emission in subcooled nucleate pool boiling. *J. Nucl. Sci. Technol.* **14**, 107–115.

PETTIGREW, M. J. & GORMAN, D. J. 1973 Experimental studies on flow induced vibration to support steam generator design. *Proc. Int. Symp. on Vibration Problems in Industry*, Keswick, England. Paper No. 424.

THIE, J. 1963 *Reactor Noise.* Rowmann & Littlefield.

VINCE, M. A. & LAHEY JR., R. T. 1980 Flow regime identification and void fraction measurement techniques in two-phase flow. NUREG/CR-1692, NTIS.

WAMBSGANSS, M. W. & ZALESKI, P. L. 1970 Measurement, interpretation and characterization of near-field flow noise. *ANL-7685*, 112–140.

WILLIAMS, M. M. R. 1974 *Random Processes in Nuclear Reactors.* Pergamon Press, Oxford.

WILLMARTH, W. W. 1975 Pressure fluctuations beneath turbulent boundary layers. *Ann. Rev. Fluid Mech.* **7**, 13–38.

YIH, T. S. & GRIFFITH, P. 1970 Unsteady momentum fluxes in two-phase flow and the vibration of nuclear system components, *Proc. of Conf. on Flow Induced Vibrations in Reactor System Components, ANL-7685*, 91–111.